The CeO_2^+ Cation: Gas-Phase Reactivity and Electronic Structure

Christoph Heinemann, Hans H. Cornehl,[†] Detlef Schröder,[†] Michael Dolg,[‡] and Helmut Schwarz*,[†]

Institut für Organische Chemie der Technischen Universität Berlin, Strasse des 17. Juni 135, D-10623 Berlin, Germany, and Max-Planck-Institut für Physik komplexer Systeme, Bayreuther Strasse 40, Haus 16, D-01187 Dresden, Germany

Received October 16, 1995[⊗]

"Bare" CeO_2^+ ions can be prepared in the gas phase by consecutive oxidation of Ce^+ with O_2 and NO_2. The ability to activate saturated and unsaturated hydrocarbons is investigated by use of Fourier-transform ion cyclotron resonance mass spectrometry. In the reactions of CeO_2^+ with linear and branched alkanes C−H bond activation is observed almost exclusively. In contrast, both oxygen-atom transfer and C−H bond activation processes occur when thermalized CeO_2^+ cations react with simple alkenes and aromatic compounds. C−C bond activation is not observed at all. Insight into the structural and electronic properties of neutral CeO_2 and cationic CeO_2^+ is provided by means of quasirelativistic density-functional and ab initio pseudopotential calculations. They reveal a $^2\Sigma_u^+$ ground state for CeO_2^+ which is best described as a linear cerium dioxide with a resonating π bond. Finally, we discuss the influence of oxo ligands on the chemistry of the cationic CeO_n^+ ($n = 0-2$) species toward hydrocarbons.

Introduction

The chemical reactivity of "bare" transition-metal cations M^+ toward various classes of substrates, with a particular emphasis on C−C and C−H bond activation of hydrocarbons, has led to a comprehensive body of information.[1] These studies have been driven by the idea to correlate the nature of chemical processes involving isolated species under well-defined conditions directly to underlying electronic and structural properties. Thus, extensive theoretical work has paralleled the experimental efforts providing deeper insight into the principles governing the reaction of a transition-metal cation M^+ with an organic substrate. Establishing a link between condensed-phase[2] and gas-phase organometallic chemistry is, however, still a formidable task.[3] A step toward bridging this gap concerns the evaluation of ligand effects; i.e. it is necessary to understand in which way a ligand L influences the reactivity of the ML^+ complex as compared to the "bare" transition-metal cation M^+.[4] With regard to oxygen ligands, recently diatomic transition-metal oxo cations MO^+ have been systematically investigated, with an emphasis on the first transition-metal row (M = Sc−Zn).[5] Not only are these species simple enough to allow an adequate treatment of their electronic structures by theoretical methods,[6] moreover, they may serve as models for more complex systems in which transition-metal oxo species appear in reaction centers in the active sites of natural and artificial catalysts.[7]

A further logical step in this development deals with the study of cationic transition-metal dioxides MO_2^+. Since MO_2^+ species can be traced back to the reaction of M^+ with dioxygen, these studies also adress the timely topic of activation of molecular oxygen.[8] The limited number of investigations available for ionic metal dioxides[5,9] has already demonstrated that at the molecular level; one does not observe simply additive ligand effects[10] when comparing M^+, MO^+, and MO_2^+. More precisely, the MO_2^+ systems have been recognized as quite complicated due to the possible existence of different isomers

[†] Techniche Universität Berlin.
[‡] Max-Plank-Institut für Physik komplexer Systeme.
[⊗] Abstract published in *Advance ACS Abstracts,* March 15, 1996.

(1) Recent reviews: (a) Armentrout, P. B. *Annu. Rev. Phys. Chem.* **1990**, *41*, 313. (b) Martinho Simões, J. A.; Beauchamp, J. L. *Chem. Rev.* **1990**, *90*, 629. (c) Eller, K.; Schwarz, H. *Chem. Rev.* **1991**, *91*, 1121. (d) Weisshaar, J. C. *Acc. Chem. Res.* **1993**, *26*, 213. (e) Freiser, B. S. *Acc. Chem. Res.* **1994**, *27*, 353.
(2) For a recent review of C−H bond activation by the help of organometallic complexes in homogeneous solution, see: Arndtsen, B. A.; Bergman, R. G.; Mobley, T. A.; Peterson, T. H. *Acc. Chem. Res.* **1995**, *28*, 154.
(3) See, for example, the discussion in: (a) Carter, E. A.; Goddard, W. A., III. *J. Phys. Chem.* **1988**, *92*, 5679. (b) Perry, J. K.; Ohanessian, G.; Goddard, W. A., III. *Organometallics* **1994**, *13*, 1870.
(4) For a spectacular example in the case of Fe^+, see: (a) Tjelta, B. L.; Armentrout, P. B. *J. Am. Chem. Soc.* **1995**, *117*, 5531. (b) van Koppen, P. A. M.; Bushnell, J. E.; Kemper, P. R.; Bowers, M. T. *J. Am. Chem. Soc.* **1995**, *117*, 2098.
(5) For a review on this area, see: Schröder, D.; Schwarz, H. *Angew. Chem., Int. Ed. Engl.* **1995**, *34*, 1973.
(6) (a) Carter, E. A.; Goddard, W. A., III *J. Phys. Chem.* **1988**, *92*, 2109. (b) Hippe, D.; Peyerimhoff, S. D. *Mol. Phys.* **1992**, *76*, 293. (c) Fiedler, A.; Hrušák, J.; Koch, W.; Schwarz, H. *Chem. Phys. Lett.* **1993**, *211*, 242. (d) Fiedler, A.; Schröder, D.; Shaik, S.; Schwarz, H. *J. Am. Chem. Soc.* **1994**, *116*, 10734. (e) Shaik, S.; Danovich, D.; Fiedler, A.; Schröder, D.; Schwarz, H. *Helv. Chim. Acta* **1995**, *78*, 1393.
(7) Ortiz deMontellano, P. R. *Cyctochrome P-450: Structure, Mechanism and Biochemistry*; Plenum Press: New York, 1986.
(8) Simándi, L. I. *Dioxygen Activation and Homogeneous Catalytic Oxidation*; Elsevier: Amsterdam, 1991.
(9) (a) Clemmer, D. E.; Dalleska, N. F.; Armentrout, P. B. *Chem. Phys. Lett.* **1992**, *190*, 259. (b) Schröder, D.; Fiedler, A.; Schwarz, J.; Schwarz, H. *Inorg. Chem.* **1994**, *33*, 5094. (c) Schröder, D.; Fiedler, A.; Herrmann, W. A.; Schwarz, H. *Angew. Chem.* **1995**, *107*, 2714. (d) The theory of metal−dioxygen complexes has been recently reviewed: Bytheway, I.; Hall, M. B. *Chem. Rev.* **1994**, *94*, 639. (e) Fiedler, A.; Kretzschmar, I.; Schröder, D.; Schwarz, H. *J. Am. Chem. Soc.*, submitted for publication.
(10) (a) Jackson, T. C.; Carlin, T. J.; Freiser, B. S. *J. Am. Chem. Soc.* **1988**, *108*, 1120. (b) Irikura, K. K.; Beauchamp, J. L. *J. Am. Chem. Soc.* **1989**, *111*, 75. (c) Cassady, C. J.; McElvany, S. W. *Organometallics* **1992**, *11*, 2367.
(11) (a) Schilling, J. B.; Beauchamp, J. L. *J. Am. Chem. Soc.* **1988**, *110*, 15. (b) Sunderlin, L. S.; Armentrout, P. B. *J. Am. Chem. Soc.* **1989**, *111*, 3845. (c) Azarro, M.; Breton, S.; Decouzon, M.; Geribaldi, S. *Int. J. Mass Spectrom. Ion Processes* **1993**, *128*, 1. (d) Heinemann, C.; Schröder, D.; Schwarz, H. *Chem. Ber.* **1994**, *127*, 1807. (e) Yin, W. W.; Marshall, A. G.; Marçalo, J.; Pires de Matos, A. *J. Am. Chem. Soc.* **1994**, *116*, 8666. (f) Heinemann, C.; Goldberg, N.; Tornieporth-Oetting, I. C.; Klapötke, T. M.; Schwarz, H. *Angew. Chem., Int. Ed. Engl.* **1995**, *34*, 213. (g) Cornehl, H. H.; Heinemann, C.; Schröder, D.; Schwarz, H. *Organometallics* **1995**, *14*, 992.

0020-1669/96/1335-2463$12.00/0

and low-lying electronic states, which may influence the chemistry of these molecules even at thermal energies.

Despite the comprehensive data available on the cationic gas-phase chemistry of d-block transition-metals[1] the investigation of the f-elements in the lanthanide series has only recently been initiated.[11] Considering the growing importance of these elements in many areas of modern technology[12] (e.g. lanthanide-based polymerization catalysts[13]), a wide field of research evolves for model studies in the gas phase which provide a deeper mechanistic understanding as well as correlations of chemical reactivities with electronic structures. General trends for the reactivity of "bare" lanthanide cations toward hydrocarbons have been established independently by several groups,[11a,e,g] while ligand effects remain by and large unexplored.[5,14] Since lanthanides are known to be extremely oxophilic, the bond strengths of their cationic oxides MO^+ are much higher as compared to the oxides of the late and middle d-block elements.[9a,15,16] Thus, thermodynamic considerations prohibit cationic lanthanide and actinide monoxides to oxidize hydrocarbons via oxygen atom transfer from the metal oxide to the substrate; this also applies for the early transition-metal cations ScO^+, TiO^+, and VO^+.[17] In fact we have found that one can make use of this high oxygen affinity of the lanthanides to generate the corresponding cationic dioxides MO_2^+, which may exhibit an interesting gas-phase chemistry due to the presence of one strongly and one weakly bound oxygen ligand. Within this context CeO_2^+ is a case in point for several reasons. (*i*) In the condensed phase cerium is known to appear in varying oxidation states. (*ii*) As the first 4f-element, cerium represents a bridge between the lanthanide and the 5d-block elements, which due to the presence of relativistic effects[18] exhibit their own characteristic gas-phase behavior.[19] (*iii*) The electronic configuration of cerium renders a metal dioxide cation particularly interesting, since it is not a priori evident how the valence electrons are distributed is this species: Either cerium in the thermodynamically unfavorable formal oxidation state +V (which involves a hole in the subvalence 5p shell) or, alternatively, cerium in the oxidation state +IV and a hole in the oxygen's valence shell. The second scenario might even give rise to an asymmetric structure with the first oxygen atom doubly bonded to Ce and a second singly bonded oxygen atom at which an unpaired electron resides. (*iv*) Finally, CeO_2 forms an essential part of technologically important catalysts (e.g. the "three-way" automobile exhaust conversion system), and model studies under well-defined conditions[20] may help to understand the specific chemical role of cerium dioxide in these applications.

Our experiments, carried out under the conditions of Fourier-transform ion cyclotron resonance (FT-ICR) mass spectrometry, demonstrate that the CeO_2^+ cation is able to bring about gas-phase activation of small saturated and unsaturated hydrocarbons, in certain cases even in a catalytic manner. We report these results together with thermochemical considerations for neutral and cationic cerium dioxide CeO_2 and the corresponding oxo(hydroxy) complexes CeO(OH). In a complementary theoretical approach, the electronic structures of CeO^+ and CeO_2^+ are investigated using density-functional and ab initio pseudopotential theory with an emphasis on the role of relativistic effects.

Experimental and Theoretical Procedures

The experiments were performed with a Spectrospin-CMS-47X Fourier-transform ion cyclotron resonance (FT-ICR) mass spectrometer which is equipped with an external ion source. The instrument and its basic operation have been described in detail elsewhere.[21] Laser desorption/laser ionization (LD/LI)[22] was used to produce Ce^+ ions by focusing the beam of a Nd:YAG laser (Spectron Systems; $\lambda = 1064$ nm) onto either a piece of pure cerium metal (Heraeus, 99.9%) or a flint stone of a conventional cigarette lighter (Ce content: ca. 70%). CeO^+ ions were generated either directly, by LD/LI of a piece of a surface-oxidized cerium metal, or in the FT-ICR cell (see below), by the reaction between Ce^+ and a pulsed-in O_2/Ar mixture (ca. 1:10). An advantage of the former procedure is high ion intensities over a reasonable time (2−3 h); however, CeO^+ formed directly by LD/LI appeared to be electronically excited (see points *i*−*iii* later in this section) such that multiple thermalization steps were required prior to reactivity studies with the subsequently generated CeO_2^+ ions. Therefore, only the latter procedure was used in the experiments presented here. Ions were extracted from the ion source, transferred to the analyzer cell by a system of electrostatic potentials and lenses, decelerated, and trapped in the field of a superconducting magnet (Oxford Instruments; maximum field strength: 7.05 T). The natural isotope distribution of cerium is as follows: ^{136}Ce, 0.19%; ^{139}Ce, 0.25%; ^{140}Ce, 88.48%; ^{142}Ce, 11.08%.[23] Therefore, $^{140}Ce^+$ or $^{140}Ce^{16}O^+$ isotopes were isolated using FERETS,[24] a computer-controlled ion ejection protocol which combines frequency sweeps and single frequency pulses to optimize ion isolation. In particular, FERETS allows for straightforward ejection of ions of masses near the ion to be isolated without kinetic excitation of the latter ion (see points *i*−*iii* later in this section). Before carrying out ion/molecule reactions, thermalization of the reactant ions was afforded by collisions with pulsed-in argon (maximum pressure ca. 5×10^{-5} mbar; ca. 400 collisions). Inorganic and organic substrates were admitted to the ICR cell via leak valves at stationary pressures, which varied, depending on the efficiencies of the observed processes, between 1×10^{-8} and 50×10^{-8} mbar. In order to ensure that only ion/molecule reactions from thermalized reactant ions were

(12) (a) *Industrial Applications of Rare Earth Elements*; Gschneider, K. A., Jr., Ed.; American Chemical Society: Washington, DC, 1981. (b) Watson, P. L. In *Selective Hydrocarbon Activation—Principles and Progress*; Davies, J. A., Watson, P. L., Liebman, J. F., Greenberg, A., Eds.; VCH Publishers: New York 1990. (c) For an up-to-date review on organolanthanide chemistry, see: Schumann, H.; Meese-Marktscheffel, J. A.; Esser, L. *Chem. Rev.* **1995**, *95*, 865.

(13) (a) Jeske, G.; Lauke, H.; Mauermann, H.; Swepston, P. N.; Schumann, H.; Marks, T. J. *J. Am. Chem. Soc.* **1985**, *107*, 8091. (b) Jeske, G.; Schock, L. E.; Swepston, P. N.; Schumann, H.; Marks, T. J. *J. Am. Chem. Soc.* **1985**, *107*, 8103. (c) Jeske, G.; Lauke, H.; Mauermann, H.; Schumann, H.; Marks, T. J. *J. Am. Chem. Soc.* **1985**, *107*, 8111.

(14) Ligand effects for C−H bond activation by HoL^+ complexes: Cornehl, H. H.; Heinemann, C.; Schwarz, H. Unpublished results.

(15) The available thermochemical data on lanthanide oxides has been compiled in: Cockett, M. C. R.; Nyulászi, L.; Veszprémi, T.; Wright, T. G.; Dyke, J. M. *J. Electron Spectrosc. Relat. Phenom.* **1991**, *57*, 373.

(16) All other thermochemical data are taken from: (a) Lias, S. G.; Liebman, J. F.; Levin, R. D. *J. Phys. Chem. Ref. Data* **1984**, *13*, 695. (b) Lias, S. G.; Liebman, J. F.; Levin, R. D.; Kafafi, S. A. *NIST Standard Reference Database, Positive Ion Energetics*, Version 2.01; NIST: Gaithersburg, MD, 1994.

(17) (a) ScO^+: Tolbert, M. A., Beauchamp, J. L. *J. Am. Chem. Soc.* **1984**, *106*, 8117. (b) TiO^+: Clemmer, D. E.; Aristov, N.; Armentrout, P. B. *J. Phys. Chem.* **1993**, *97*, 544. (c) VO^+: Reference 10a. (d) ScO^+, TiO^+, VO^+: Ryan, M. F.; Stöckigt, D.; Schwarz, H. *J. Am. Chem. Soc.* **1994**, *117*, 9565.

(18) Heinemann, C.; Hertwig, R. H.; Wesendrup, R.; Koch, W.; Schwarz, H. *J. Am. Chem. Soc.* **1995**, *117*, 495.

(19) (a) Irikura, K. K.; Beauchamp, J. L. *J. Phys. Chem.* **1991**, *95*, 8344. (b) Wesendrup, R.; Schröder, D.; Schwarz, H. *Angew. Chem., Int. Ed. Engl.* **1994**, *33*, 1174. (c) Heinemann, C.; Wesendrup, R.; Schwarz, H. *Chem. Phys. Lett.* **1995**, *239*, 75.

(20) See also: (a) Bozon-Verduraz, F.; Bensalem, A. *J. Chem. Soc., Faraday Trans.* **1994**, *90*, 653. (b) Soria, J.; Martínez-Arias, A.; Conesa, J. C. *J. Chem. Soc., Faraday Trans.* **1995**, *91*, 1669.

(21) (a) Eller, K.; Schwarz, H. *Int. J. Mass Spectrom. Ion Processes* **1989**, *93*, 243. (b) Eller, K.; Zummack, W.; Schwarz, H. *J. Am. Chem. Soc.* **1990**, *112*, 621.

(22) (a) Freiser, B. S. *Talanta* **1985**, *32*, 697. (b) Freiser, B. S. *Anal. Chim. Acta* **1985**, *178*, 137.

(23) Heath, R. L. In *CRC Handbook of Chemistry and Physics*; Weast, R. C., Ed.; CRC Press: Boca Raton, FL, 1990.

(24) Forbes, R. A.; Laukien, F. H.; Wronka, J. J. *Int. J. Mass Spectrom. Ion Processes* **1988**, *83*, 23.

observed the following routine checks were performed: (*i*) The decay of the reactant ion should follow strict pseudo-first-order kinetics. (*ii*) Varying the number of thermalizing collisions of the reactant ion with the pulsed-in argon gas should change neither the observed rate constant *k* nor the product distribution. (*iii*) The intensities of exothermic product ions should continuously rise with longer trapping times, provided they do not undergo secondary reactions. The elemental composition of reaction products were determined by high-resolution mass spectrometry ($m/\Delta m \approx 200\,000$), and the reaction pathways were elucidated by MS/MS and double-resonance techniques. Rate constants *k* were determined from the pseudo-first-order decay of the reactant ion intensity and are reported with accuracies of ±25−50% (dependent on the interference of background reactions, see below) as percentages of the theoretical collision rates k_{ADO} calculated from average dipole orientation (ADO) theory.[25] Branching ratios were derived from the analysis of the initial slopes of the product ion intensities and are reproducible within ±20%. Collision-induced dissociation (CID) experiments[26] were carried out by (*i*) isolation of the desired ion using FERETS, (*ii*) kinetic excitation of this ion by a radio-frequency pulse, and (*iii*) trapping it for 1 s in argon at a static pressure of 2×10^{-8} mbar. All functions of the mass spectrometer were controlled by a Bruker Aspect 3000 minicomputer.

CeO_2^+ was generated from CeO^+ and NO_2 (see below) which was pulsed into the ICR cell in a 1:5 mixture with argon so that for ca. 0.5 s the pressure in the cell rose to ca. 5×10^{-6} mbar. Subsequently, a delay of 3−5 s was applied for removal of the reactant gas. Unfortunately, it is not possible to pump-off NO_2 completely within this interval, and even longer delays (up to 10 s) were insufficient and only lead to an undesired loss of ion intensity. Thus, the remaining NO_2 gas had to be considered as background contamination during the ion/molecule reactions which has the following consequences: (*i*) The product ion CeO^+, resulting from an eventual reduction of CeO_2^+ is reoxidized to CeO_2^+ in a secondary process. (*ii*) Even if no reactants which transfer a hydrogen atom to CeO_2^+ were admitted to the cell, some CeO_2H^+ is observed from the reaction of CeO_2^+ with hydrocarbon contaminants which are inevitably present in the pulsed-in NO_2 gas due to deterioration of rubber seals in the valves and the inlet system by NO_2. $CeO_2H_2^+$ is formed as second sideproduct with the background. Whenever CeO_2H^+ was observed as a reaction product, it was checked that the ion originated from the reaction of CeO_2^+ with the reactant gas and not with background contaminants by performing a blind-probe experiment with argon as "reactant" and by verifying that the observed intensity of CeO_2^+ decreased according to the required first-order law. The reported rate constants and branching ratios are corrected for the formation of $CeO_2H_n^+$ ($n = 1,2$) from the background reaction.

The density-functional[27] calculations were performed using the Amsterdam density-functional code (ADF, version 1.1.2[28]). The employed functional was the local-density approximation (LDA) in the Vosko−Wilk−Nusair parametrization on the homogeneous electron gas with Becke's (B) and Perdew's (P) gradient corrections to the exchange and correlation parts (included during the self-consistent procedure); this will be denoted LDA+BP.[29] The adjustable parameter controlling the accuracy of the numerical integration[28b] was set to 5.0. Uncontracted Slater-type basis functions were used for the LCAO-MO expansion. In detail, triple-ζ quality basis sets were employed to describe the 4f and 5d orbitals of cerium, the 1s orbital of hydrogen, and the 2s and 2p orbitals of oxygen, while double-ζ quality was chosen for the 5s, 5p, and 6s orbitals of cerium. For the description of polarization effects, two p- and one d-functions were used for hydrogen, one d- and one f-functions for oxygen, and a single p-function for cerium (total of 97 Slater-type orbitals for CeO_2). A further characteristic feature of the employed implementation are Slater-type fit-functions for the evaluation of the Coulomb potential and a frozen-core approximation[30] (2s and 2p electrons explicitly considered for O; 5s, 5p, 4f, 6s, and 6p for Ce). In the quasirelativistic calculations, core potentials for the description of the relativistic effects in the core shells were generated with the auxiliary program DIRAC.[28c] The scalar quasirelativistic wave functions were obtained by adding the Darwin and mass−velocity operators to the Hamiltonian and diagonalizing this operator in the space of the zero-order (i.e. nonrelativistic) solutions.[31] All nonrelativistic and quasirelativistic geometries were optimized stepwise by calculating several points in the proximity of the minima on the potential-energy surfaces.

The density-functional calculations were supplemented by quasirelativistic ab initio pseudopotential (PP) self-consistent field (SCF), complete active space multiconfiguration SCF (MCSCF) with subsequent single-reference and multireference configuration interaction (CISD, MRCI), and averaged coupled pair-functional (ACPF) calculations. Single-point coupled-cluster calculations including all single and double excitations as well as a perturbative treatment of triple excitations (CCSD(T)) were performed for some cases.[32] All MRCI results reported here were obtained with a reference space consisting of 13 active orbitals for 24 electrons (in D_{2h} symmetry; $4a_g + b_{1g} + 2b_{1u} + 3b_{2u} + b_{3g} + 2b_{3u}$; in C_{2v} symmetry, $6a_1 + 2b_1 + 4b_2 + a_2$). The Langhoff-Davidson size-consistency correction[33] was included in all CI calculations. These calculations were performed with the COLUMBUS[34] and MOLPRO[35] program systems. For Ce, a 30 valence electron PP (1s−3d treated as core orbitals) and a (12s11p10d9f2g)/[8s7p6d5f2g] Gaussian-type orbital valence basis set was used,[36] whereas oxygen was treated at the all-electron level with a (9s6p2d)/[5s3p2d] basis set. The segmented contraction scheme was used throughout; this procedure will be referred to as basis set A. Since metal oxides exhibit nonnegligible intramolecular charge transfer, an accurate description of the atomic oxygen anion is required. Therefore, in a seond series of calculations we used a correlation-consistent polarized valence triple-ζ basis (cc-pVTZ) set for O,[37] augmented by one diffuse s, p, d, and f function,[38] respectively. This (11s6p3d2f)/[5s4p3d2f] basis uses the generalized contraction scheme and will be denoted as basis set B. The ACPF electron affinities of O are 0.94 and 1.22 eV for basis A and B ($1s^2$ core kept frozen), respectively, and the corresponding density functional (LDA+BP) result is 1.57 eV (experimental value 1.46 eV[39]). In order to estimate the effects of spin−orbit coupling, additional

(25) Su, T.; Bowers, M. T. *Int. J. Mass Spectrom. Ion Phys.* **1973**, *12*, 347.
(26) (a) Cody, R. B.; Burnier, R. C.; Freiser, B. S. *Anal. Chem.* **1982**, *54*, 96. (b) Jacobson, D. B.; Freiser, B. S. *J. Am. Chem. Soc.* **1983**, *105*, 5197.
(27) (a) Parr, R. G.; Yang, W. *Density-Functional Theory of Atoms and Molecules*; Oxford University Press: New York, 1989. (b) March, N. H. *Electron Density Theory of Atoms and Molecules*; Academic Press: London, 1992. For excellent reviews, see: (c) Gunnarsson, G.; Jones, R. G. *Rev. Mod. Phys.* **1989**, *61*, 689. (d) Ziegler, T. *Chem. Rev.* **1991**, *91*, 651.
(28) (a) Baerends, E. J.; Ellis, D. E. *Chem. Phys.* **1973**, *2*, 71. (b) teVelde, B.; Baerends, E. J. *J. Comput. Phys.* **1992**, *99*, 84, and references cited therein. (c) *ADF User's Manual*, Version 1.1.2; Vrije Universität: Amsterdam, 1994.
(29) (a) Vosko, S. H.; Wilk, L.; Nusair, M. *Can. J. Phys.* **1980**, *58*, 1200. (b) Perdew, J. P. *Phys. Rev. B* **1986**, *33*, 8822. (c) Becke, A. D. *Phys. Rev. A* **1988**, *38*, 3098.
(30) Snijders, J. G.; Baerends, E. J. *Mol. Phys.* **1977**, *33*, 1651.
(31) (a) Ziegler, T.; Tschinke, V.; Baerends, E. J.; Snijders, J. G.; Ravenek, W. *J. Phys. Chem.* **1989**, *93*, 3050. Recent applications of this scheme: (b) Reference 18. (c) Heinemann, C.; Schwarz, H. *Chem.—Eur. J.* **1995**, *1*, 7. (d) Hrušák, J.; Hertwig, R. H.; Schröder, D.; Schwerdtfeger, P.; Koch, W.; Schwarz, H. *Organometallics* **1995**, *14*, 1284.
(32) For reviews of these methods to describe electron correlation, see: (a) MCSCF and CI methods: Roos, B. O.; Siegbahn, P. E. M. In *Lecture Notes in Chemistry*; Roos, B. O., Ed., Springer: Berlin, Heidelberg, Germany, New York, Tokyo, 1992; Vol. 58. (b) CCSD(T) methods: Bartlett, R. J.; Stanton, J. F. In *Reviews in Computational Chemistry*; Lipkowitz, K. B., Ed., VCH: New York, 1994; Vol. 5.
(33) Langhoff, S. R.; Davidson, E. R. *Int. J. Quantum Chem.* **1974**, *8*, 61.
(34) Program system COLUMBUS: Shepard, R.; Shavitt, I.; Pitzer, R. M.; Comeau, D. C.; Pepper, M.; Lischka, H.; Szalay, P. G.; Ahlrichs, R.; Brown, F. B.; Zhao, J.-G. *Int. J. Quantum Chem. Symp.* **1988**, *22*, 149.
(35) Program system MOLPRO: (a) Knowles, P. J.; Werner, H.-J. *Chem. Phys. Lett.* **1985**, *115*, 5053. (b) Knowles, P. J.; Werner, H.-J. *Chem. Phys. Lett.* **1988**, *145*, 514. (c) Werner, H.-J.; Knowles, P. J. *J. Chem. Phys.* **1988**, *89*, 5803. (d) Werner, H.-J.; Knowles, P. J. *Theor. Chim. Acta* **1990**, *78*, 175.
(36) (a) Dolg, M.; Stoll, H.; Preuss, H. *J. Chem. Phys.* **1989**, *90*, 1730. (b) Igel-Mann, G.; Stoll, H.; Preuss, H. *Mol. Phys.* **1988**, *65*, 1321.
(37) Dunning, T. H. *J. Chem. Phys.* **1989**, *90*, 1007.
(38) Kendall, R. A.; Dunning, T. H.; Harrison, R. J. *J. Chem. Phys.* **1992**, *96*, 6796.
(39) Hotop, H.; Lineberger, W. C. *J. Phys. Chem. Ref. Data* **1975**, *4*, 539.

Scheme 1

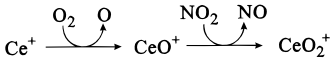

Scheme 2

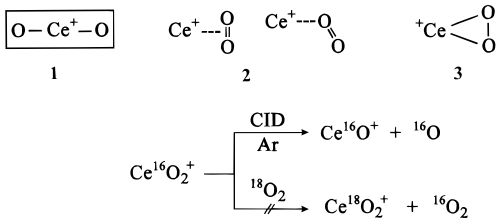

calculations were carried out with the COLUMBUS spin−orbit CI program.[40] In addition to the 30 valence electron PP and a corresponding spin−orbit operator for Ce, a 6 valence electron PP[36b] was used for O. Generally contracted (11s10p9d8f)/[4s3p3d2f] and (5s5p)/[2s2p] basis sets of valence double-ζ quality were applied for Ce and O, respectively (basis set C). Due to limitations of the basis sets and correlation treatments, these calculations are only used to extract spin−orbit contributions, which are then added to the results obtained with the larger basis sets A and B in the better correlated calculations without spin−orbit interaction.

Results and Discussion

The paper is organized in the following way: First, we will present the experimental results, i.e. the generation of CeO_2^+, discuss its structural features, present the reactivity studies, and analyze some thermochemical implications of these experiments. The second part is devoted to theoretical investigations of CeO_2^+. Finally, the different gas-phase reactivities of Ce^+, CeO^+, and CeO_2^+ toward hydrocarbons will be compared in light of the theoretical results.

I. Generation and Structure of CeO_2^+. CeO_2^+ is readily generated under FT-ICR conditions as the single product of the ion/molecule reaction between CeO^+ and nitrogen dioxide (Scheme 1). Other common oxidation reagents, such as N_2O, O_2, or NO, do not serve as oxygen donors and were found to be unreactive toward CeO^+. However, with the "bare" Ce^+ cation, these three oxidants as well as NO_2 promote the rapid formation of CeO^+; in the Ce^+/N_2O reaction, CeN^+ evolves as an additional product ($CeO^+/CeN^+ = 2:1$).

Basically, three different types of connectivities are conceivable for the CeO_2^+ molecule:[9b,c] the cerium dioxide type **1**, an adduct complex of Ce^+ with an intact dioxygen molecule (side-on or end-on) **2**, or a cationic cerium dioxirane **3** (see Scheme 2). On the basis of collision-induced dissociation (CID) and isotope labeling experiments, it appears that CeO_2^+, generated as described in Scheme 1, corresponds to a genuine cerium dioxide, **1**. This conclusion is based on the following observations: Upon CID, exclusive loss of a single oxygen atom from CeO_2^+ with concomitant generation of CeO^+ is observed (Scheme 2). Within the chosen energy regime (max. 100 eV center-of-mass collision energy) no signal for Ce^+ occurs, thus rendering structures **2** or **3**, for which also loss of an intact O_2 moiety would be expected, unlikely. Furthermore, $Ce^{16}O_2^+$ does not undergo any ligand exchange reaction with $^{18}O_2$ (see Scheme 2). Thus, a complex of Ce^+ with molecular oxygen (**2**) can be excluded since no substantial kinetic barrier for the corresponding thermoneutral ligand exchange process is expected. The same argument also applies for structure **3**. Fully in line with the expected behavior of **1**, both oxo ligands are found to be equivalent in chemical reactions and collision-induced dissociation: First, oxidation of ethene (see below) by $Ce^{18}O^{16}O^+$, which can be generated by a primary reaction of Ce^+ with $^{18}O_2$ followed by secondary oxidation of the resulting $Ce^{18}O^+$ cation with $N^{16}O_2$ (Scheme 3), yields $Ce^{16}O^+$ and $Ce^{18}O^+$ in identical intensities. Second, in the CID of $Ce^{18}O^{16}O^+$, the products $Ce^{18}O^+$ and $Ce^{16}O^+$ are observed in equal amounts with concomitant losses of the neutral oxygen atoms ^{16}O and ^{18}O (Scheme 3).

Scheme 3

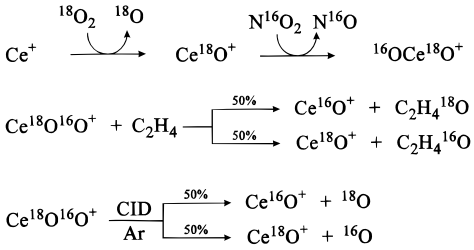

The *exothermic* formation of CeO_2^+ from CeO^+ and NO_2 marks a sharp contrast to the chemical behavior of the related d-block element oxides ScO^+, YO^+, and LaO^+, for which the analogous reactions are *endothermic* by 32 ± 4, 32 ± 4, and 48 ± 7 kcal/mol, respectively.[9a] In a very simple picture, one can relate the fact that the reaction becomes energetically more favorable in the case of cerium to the ground state electronic configurations of related MO^+ cations: The group 3 oxocations ScO^+, YO^+, and LaO^+ exhibit closed shell ground states[41] ($^1\Sigma^+$), in which the two valence electrons of the transition-metal cation are involved in making the strong covalent bonds to the oxygen ligand. As discussed by Armentrout and co-workers,[9a,42] additional back-donation from the oxygen lone-pair electrons into empty s- and d-orbitals of the transition-metal cation can be inferred from the high bond-dissociation energies (BDEs) of the group 3 oxocations. Thus, the bonding interaction in these diatomic molecules can be formally characterized as a triple bond between oxygen and the metal. Consequently, a second oxygen atom ligand perturbs an electronically very stable situation such that the resulting BDEs of the second oxygen to the MO^+ unit are small. However, in CeO^+ an additional electron occupies a nonbonding 4f orbital. Upon formation of the second cerium−oxygen bond, this electron becomes involved in chemical bonding such that CeO_2^+ is expected to be energetically more stabilized as compared to MO_2^+ species of the group 3 metals. In fact, the observation of an oxygen atom transfer from NO_2 to CeO^+ implies that BDE (OCe^+-O) exceeds BDE ($ON-O$), which amounts to 73 kcal/mol.[16] We briefly note here that earlier experimental observations of CeO_2^+ have been reported in mass-spectrometric studies using electron impact ionization of gaseous CeO_2 molecules evaporated from solid CeO_2 samples[43] and in the chemiionization reaction between neutral cerium atoms and O_2 ($Ce + O_2 \rightarrow CeO_2^+ + e^-$);[44] thermochemical implications of these studies will be compared to the present investigation further below.

II. Chemical Reactivity of CeO_2^+. Two general reaction patterns are observed, if CeO_2^+ is subjected to ion/molecule

(40) Chang, A.; Pitzer, R. M. *J. Am. Chem. Soc.* **1989**, *111*, 2500.

(41) Márquez, A.; Capitán, M. J.; Odriozola, J. A.; Sanz, J. F. *Int. J. Quant. Chem.* **1994**, *52*, 1329.

(42) Fisher, E. R.; Elkind, J. L.; Clemmer, D. E.; Georgiadis, R.; Loh, S. K.; Aristov, N.; Sunderlin, L. S.; Armentrout, P. B. *J. Chem. Phys.* **1990**, *93*, 2676.

(43) (a) Stanley, H. G.; Norman, J. H. *Int. J. Mass Spectrom. Ion Phys.* **1969**, *2*, 35. (b) Ackerman, R. J.; Rauh, E. G. *J. Chem. Thermodyn.* **1971**, *3*, 609. (c) Kordis, J.; Gingerich, K. A. *J. Chem. Phys.* **1977**, *66*, 483. (d) Piacente, V.; Bardi, G.; Malaspina, L.; Desideri, A. *J. Chem. Phys.* **1973**, *59*, 31.

(44) Cockett, M. C. R.; Dyke, J. M.; Ellis, A. M.; Fehér, M.; Wright, T. G. *J. Electron Spectrosc. Relat. Phenom.* **1990**, *52*, 529.

Table 1. Observed Rate Constants k_{obs}[a] for Reactions of CeO_2^+ with Selected Organic Substrates Relative to the Theoretical Collision Rate k_{ADO}[25]

substrate	k_{obs}/k_{ADO}	substrate	k_{obs}/k_{ADO}
CH_4	< 0.0001	C_3H_6	0.44
C_2H_6	< 0.0001	1-C_4H_8	0.62
C_3H_8	0.003[b]	C_4H_6	0.80
i-C_4H_{10}	0.04	C_6H_6	0.64
n-C_4H_{10}	0.10	C_6H_5Cl	0.65
$C(CH_4)_3$	0.03	C_6H_5F	0.45
c-C_6H_{12}	0.35	$C_6H_5CH_3$	0.55
C_2H_4	0.10		

[a] Absolute uncertainties ±30%. [b] Absolute uncertainty ±50% due to very slow reaction and possible interferences from background contaminants.

Scheme 4

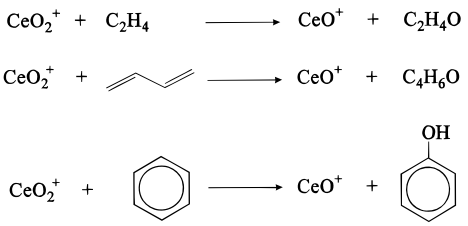

Scheme 5

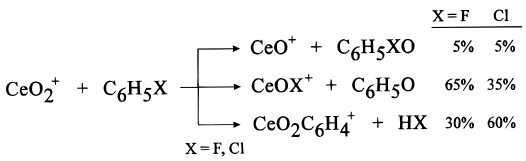

reactions with hydrocarbons: (*i*) oxygen-atom transfer from CeO_2^+ to the substrate and concomitant formation of CeO^+ and (*ii*) abstraction of hydrogen atoms from the hydrocarbon leading to either CeO_2H^+ and a neutral hydrocarbon radical or $CeO_2H_2^+$ and an alkene. We will now discuss the typical substrates for which these pathways are observed. The measured rate constants are given in Table 1.

(a) Unsaturated substrates such as ethene, 1,3-butadiene, and benzene are readily oxidized by CeO_2^+ (see Scheme 4). In these three cases, oxygen transfer from the metal to the hydrocarbon constitutes the only observed reaction pathway (except for electron transfer in the case of 1,3-butadiene,[45] see below); there is no indication for C−C bond activation or hydrogen abstraction reactions. However, when passing to substituted benzenes, namely fluoro- and chlorobenzene, in addition to the oxidation reaction also C−X (X = F, Cl) bond activation, loss of an HX molecule, as well as electron transfer[45] (see below), takes place (Scheme 5).

The reaction of CeO_2^+ with the simplest olefin, namely ethene, proceeds at only 10% of the theoretical collision rate k_{ADO} (Table 1). For larger substrates the corresponding processes are kinetically more efficient (80% of k_{ADO} for 1,3-butadiene, 64% for benzene). This is expected since at the energy level of the entrance channel the density of states of the rovibrationally excited encounter complexes, and thus its lifetime, becomes larger with increasing size and polarizabilities of the neutral reactant. The nature of the oxidation product in the CeO_2^+/ethene reaction cannot be inferred from known

Scheme 6

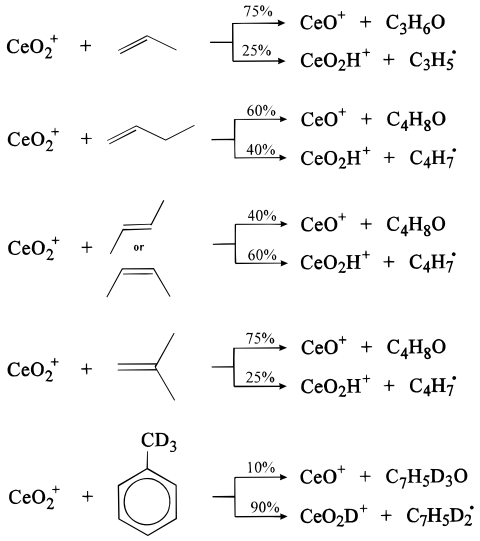

thermochemical data,[16] since exothermic generation of acetaldehyde CH_3CHO, its tautomer vinyl alcohol $H_2C{=}CH(OH)$, or oxirane is compatible with the lower limit of 73 kcal/mol for the strength of the $OCe^+{-}O$ bond as derived above. Even worse, for CeO_2^+/1,3-butadiene the thermochemical data[16] render not fewer than 19 isomeric C_4H_6O products energetically feasible. Similarly, oxygen-atom transfer from CeO_2^+ to benzene may lead to various products of which phenol is not only the global energetic minimum but also mechanistically conceivable.[46] In addition to the transfer of an oxygen atom two further primary processes are observed in the reactions of the two substituted benzenes C_6H_5X (X = F, Cl) with CeO_2^+: An oxygen-ligand of CeO_2^+ is substituted by a halogen atom resulting in the generation of the mixed oxygen/halogen complexes $OCeX^+$ and loss of $C_6H_5O^\bullet$ (most likely a phenoxy radical). Moreover, one observes loss of HX with the concomitant formation of a $CeO_2C_6H_4^+$ complex, for which a catechol structure seems reasonable; however, this structure is not subject of the current study. The C−F and C−Cl bond activation processes can be accounted for by the thermochemical driving force for the formation of strong lanthanide−halogen bonds. Similar observations have recently been reported for the reactions of bare and ligated praseodymium cations Pr^+ with several fluorine-substituted hydrocarbons.[11f]

In addition to the ligand exchange and oxidation reactions, 1,3-butadiene and chlorobenzene transfer an electron to CeO_2^+ resulting in the formation of the respective radical cations as well as neutral CeO_2. Yet, these charge transfer pathways are minor as compared to the competing reactions described above (<5% of all ionic products). No electron transfer was observed between properly thermalized CeO_2^+ and benzene.

(b) Scheme 6 provides an overview of the reactions of CeO_2^+ with higher olefins as well as toluene. Here, the oxidation pathway via oxygen atom transfer has to compete with formation of CeO_2H^+, most probably due to homolytic fission of the weak allylic or benzylic C−H bonds in these substrates. The measured relative reaction rates (44% of k_{ADO} for propene, 62% of k_{ADO} for 1-butene, and 55% of k_{ADO} for toluene) reflect again the larger attractive interactions in the ion/molecule complex when the size of the hydrocarbon substrate is increased. The branching ratios between the two observed reaction channels

(45) For reasons of clarity, electron transfer processes are not depicted in the schemes. Moreover, branching ratios are evaluated relative to all major processes. Electron transfer pathways are not included, since in all cases where they are observed they account to less than 5% of all ionic products.

(46) (a) Schröder, D.; Schwarz, H. *Helv. Chim. Acta* **1992**, *75*, 1281. (b) Becker, H.; Schröder, D.; Zummack, W.; Schwarz, H. *J. Am. Chem. Soc.* **1994**, *116*, 1096.

Scheme 7

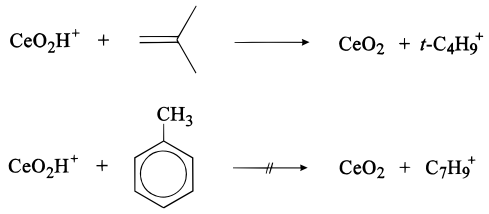

exhibit a somewhat irregular trend showing predominant oxidation for propene, 1-butene, and isobutene, while for the two stereoisomeric 2-butenes H-atom abstraction prevails. For toluene, abstraction of the *benzylic* hydrogen atom, as evidenced by the formation of CeO_2D^+ from CeO_2^+ and $C_6H_5CD_3$, is the dominant process. Still, oxygen transfer is observed as a minor product (10%) as well as electron transfer[45] (<5%) resulting in the formation of $C_7H_8^{+\bullet}$ and neutral CeO_2. Thermochemically, this is in line with the observed charge transfer from chlorobenzene (IE = 9.07 eV[16]), which has a larger ionization energy than toluene (IE = 8.82 eV[16]). Unfortunately, the possible isomeric products of O-atom transfer to toluene and the olefins cannot be deduced from thermochemical data.[16] For example, in the case of CeO_2^+/propene, five different oxidation products are thermochemically allowed and for CeO_2^+/1-butene even 21 different oxidation products may be formed, if the reaction is required only to be exothermic.

As far as secondary reactions are concerned, it is instructive that only isobutene undergoes subsequent proton transfer with initially formed CeO_2H^+ cations to yield *t*-$C_4H_9^+$ and neutral CeO_2, respectively (see Scheme 7). No reaction was, however, observed between CeO_2H^+ and toluene as well as all other substrates with a lower proton affinity than toluene. Under the reasonable assumption that no activation barrier exists for the transfer of a proton from CeO_2H^+ to the organic substrates, these reactions provide thermochemical information on the heat of formation of CeO_2H^+ (see below). From the structural point of view, this species represents most likely a mixed oxo(hydroxy) complex $OCe(OH)^+$; this assumption is consistent with the high-energy collisional activation (CA) spectrum obtained of CeO_2H^+ ions generated by fast-atom bombardment of aqueous Ce(IV) ions:[47] Here, one observes preferential fragmentation to CeO^+ (rel. abundance 100%), together with minor channels leading to CeO_2^+, Ce^+ and $CeOH^+$ (rel. abundances of 15, 10, and 5%, respectively). In addition, small fractions of doubly charged CeO^{2+} and Ce^{2+} ions are produced in this process. This fragmentation pattern is not expected for the hydrido dioxo species $HCe(O)_2^+$ or the hydroperoxide isomer $Ce(OOH)^+$.

(c) The observed reactions of CeO_2^+ with small linear, branched, and cyclic alkanes are displayed in Scheme 8. Both methane and ethane are not activated by CeO_2^+ under our experimental conditions. Typical for larger alkanes is C−H bond activation resulting in formation of CeO_2H^+ and a neutral hydrocarbon radical. These processes are kinetically quite inefficient as compared to the corresponding reactions involving partially unsaturated hydrocarbons (see above). For example,

Scheme 8

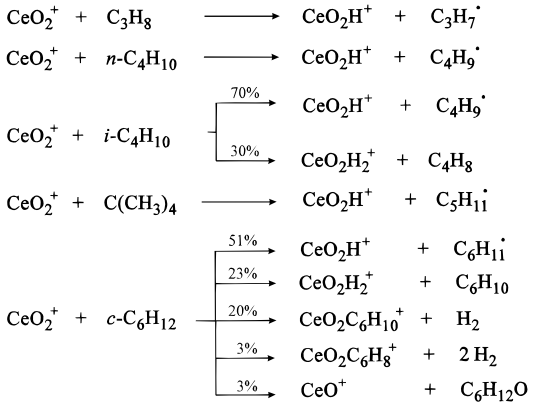

propane reacts only in 0.3% of all collisions and the respective rates increase slowly along the sequence neopentane, isobutane, *n*-butane, and cyclohexane. For the branched C_4H_{10} isomer and cyclohexane, a second primary product channel is observed, namely transfer of two hydrogen atoms with formation of $CeO_2H_2^+$. Unfortunately, a structural distinction between the two possible isomers, i.e. the mixed oxy−water complex $OCe^+-(OH_2)$ and the bis(hydroxy) species $Ce(OH)_2^+$, could not be accomplished due to the ambiguity of the CA spectrum of $[Ce,O_2,H_2]^+$ (relative abundances: CeO^+, 100%; $CeOH^+$, 20%; Ce^+, 10%; $[Ce,O_2,H]^+$, 10%, $[Ce,O,H_2]^+$, 2%).[47] However, we suspect than these two structures are close in energy (both involve the +III oxidation state of cerium and an equal number of formal Ce−O and O−H bonds) such that with the expected low barrier for hydrogen migration their interconversion may take place on short time scales within the accessible energy regime of the FT-ICR experiments. Eventually, $CeO_2H_2^+$ is observed in all systems considered here, as it is formed in the secondary reactions between CeO_2H^+ and the saturated hydrocarbon substrates; note that due to the low reaction rates and possible background interferences, branching ratios for primary formation of $CeO_2H_2^+$ below 5% cannot be excluded.

The CeO_2^+/cyclohexane system exhibits one major and two minor additional reaction patterns which were not observed for the other alkanes considered here: loss of one (20%) or two (3%) H_2 molecules from the substrate with formation of $CeO_2C_6H_n^+$ ($n = 10, 8$) and oxidation of the hydrocarbon under generation of CeO^+ (3%). On a gross scale, the observed reactivity pattern between CeO_2^+ and alkanes can be explained by the increasing polarizability of the substrates.[11] A more detailed discussion of the underlying mechanisms requires additional thermodynamic and theoretical information as will be presented in section VI of this paper. Finally, we would like to mention that with incompletely thermalized CeO_2^+ cations a third reaction pathway with alkanes was also observed, namely hydride transfer with formation of $C_nH_{2n+1}^+$ cations and neutral CeO_2H. However, these channels, which appear to lie only slightly above the energy threshold of the FT-ICR experiment, disappeared after a careful reoptimization of the isolation and thermalization sequence for the CeO_2^+ reactant.

III. Catalytic Oxidation of Ethene. The presence of NO_2 in the background of the FT-ICR cell (see Experimental and Theoretical Procedures) allows the observation of a *catalytic* gas-phase oxidation of ethene mediated by CeO_2^+, provided that the experimental parameters are chosen properly. Figure 1 displays the relative intensities of the CeO_2^+, CeO^+ and CeO_2H^+ ions over 60 s at a static C_2H_4 pressure of 1×10^{-7} mbar and NO_2/Ar mixtures pulsed-in up to a pressure of 1×10^{-5} mbar for ca. 1 s.

(47) This experiment was carried out in a sector-field mass spectrometer of BEBE configuration. Briefly, CeO_2H^+ and $CeO_2H_2^+$ ions were generated by fast-atom bombardment of $Ce(SO_4)_2$ from an aqueous matrix, accelerated to 8 keV kinetic energy and mass- as well as energy-selected using B(1) and E(1). He (80% transmission) was used to induce collisional activation of these ions and fragments were recorded by scanning B(2). For a description of the machine, see: (a) Srinivas, R.; Sülze, D.; Weiske, T.; Schwarz, H. *Int. J. Mass Spectrom. Ion Processes* **1990**, *107*, 369. (b) Srinivas, R.; Sülze, D.; Koch, W.; DePuy, C. H.; Schwarz, H. *J. Am. Chem. Soc.* **1991**, *113*, 5970.

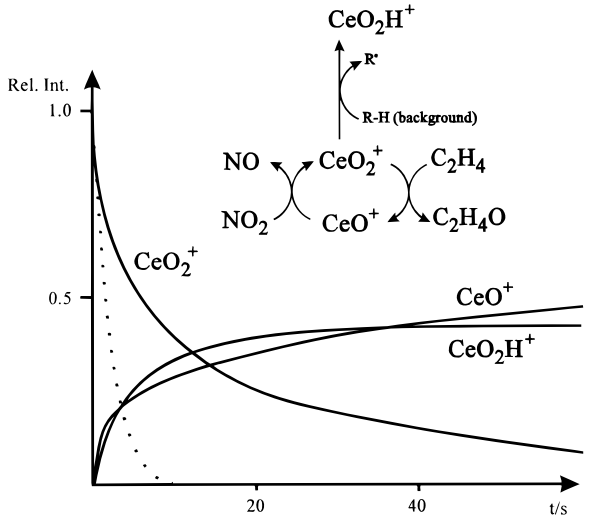

Figure 1. Catalytic oxidation of ethene by CeO_2^+: reaction scheme and time dependency of the relative ion intensities of CeO_2^+, CeO^+, and CeO_2H^+. The dotted line shows the decay of the CeO_2^+ signal for the noncatalytic reaction (i.e. if CeO^+ was not continuously reoxidized) extrapolated from the initial slope of the effectively measured decay.

The rate constant for the initial oxidation of C_2H_4 by CeO_2^+ amounts to ca. 1×10^{-10} cm^3 s^{-1} molecule^{-1} (Table 1), and the extrapolated first-order decay of the CeO_2^+ intensity according to this rate is shown by the dotted line in Figure 1. What one actually observes is a much slower decay for the CeO_2^+ intensity (solid line) which is due to reoxidation of CeO^+ by NO_2 from the background. Thus, the kinetic data demonstrate that CeO_2^+ catalyzes the gas-phase oxidation of C_2H_4 by NO_2. Since O-atom transfer corresponds to the only product channel in the reaction of CeO_2^+ with ethylene, the reaction is in principle fully catalytic since no cerium-containing ions are lost from the catalytic cycle by side reactions. Under the experimental conditions, however, the average number of cycles per molecule CeO_2^+ (turnover rate) is limited to 8 for the following reasons: At first, the residual NO_2 is gradually pumped away from the FT-ICR cell over the time of the catalytic reaction and, more importantly, CeO_2^+ reacts with hydrocarbon contaminants present in the pulsed-in NO_2 to generate CeO_2H^+, which is unreactive toward ethylene. However, also these contaminants are pumped off the cell during the reaction which leads to three different stages in the experiment shown in Figure 1: (*i*) In the first 2 s one observes mainly the primary oxidation of C_2H_4 by CeO_2^+ as well as reaction of CeO_2^+ with the contaminants to form CeO_2H^+, as evident from the steep decay of the CeO_2^+ intensity and increase of the CeO^+ and CeO_2H^+ intensities. (*ii*) In the time window 2 s $< t <$ 30 s, reoxidation of CeO^+ to CeO_2^+ becomes significant, which causes the CeO^+ concentration to rise less rapidly. (*iii*) At $t \approx$ 30s the hydrocarbon contaminants have been pumped away, which causes the CeO_2H^+ intensity to reach a plateau. NO_2 is still present in the background of the experiment to some extent and one observes exclusively the catalytic oxidation. However, even the remaining NO_2 is gradually pumped away such that the CeO_2^+ intensity eventually approaches zero. The present finding is yet another example for catalytic oxidation processes in the gas phase[48] and demonstrates the unique potential of FT-ICR mass spectrometry for the detailed investigation of complex reaction sequences under well-defined conditions.

Scheme 9

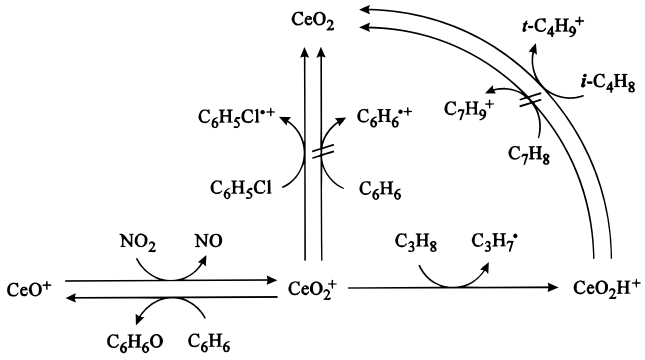

IV. Thermochemical Data. In an FT-ICR setup, thermochemical data can be deduced from the observation of ion/molecule reactions by employing the "bracketing" technique.[49] Provided that the ions of interest are properly thermalized, only exothermic or thermoneutral reactions can occur.[50] The starting point for the derivation of heats of formation for CeO_2, CeO_2^+, and CeO_2H^+ is the heat of formation ($\Delta_F H$) for CeO^+, as derived from the heat of formation (101 kcal/mol)[16] and the ionization energy (IE) of the cerium atom (5.54 eV),[51] and the BDE and IE of the neutral cerium monoxide, for which we use the values and uncertainty bars recommended by Dyke and co-workers (BDE(CeO) = 189 ± 5 kcal/mol; IE(CeO) = 5.2 ± 0.5 eV).[15] Thus, one arrives at $\Delta_F H(CeO^+) = 91 \pm 16$ kcal/mol.

An overview of the experiments leading to the thermochemical data derived here is given in Scheme 9. Formation of CeO_2^+ from oxidation of CeO^+ by NO_2 leads to a lower bound of BDE (OCe^+-O) > 73 kcal/mol, whereas the exothermic oxidation of benzene by CeO_2^+ requires BDE(OCe^+-O) < 102 kcal/mol if formation of the thermodynamically most stable C_6H_6O isomer (phenol) is assumed. These results bracket BDE(OCe^+-O) as 88 ± 15 kcal/mol, less than half the strength of the first Ce^+-O bond, 197 ± 17 kcal/mol. Thermochemical information for CeO_2H^+ is available from the hydrogen-transfer reactions: Propane is the smallest alkane, in which CeO_2^+ induces homolytic C−H bond cleavage; thus the lower limit for BDE(CeO_2^+-H) amounts to 99 kcal/mol, according to the BDE of the secondary C−H bonds. A direct determination of an upper bound for BDE ($OCeO^+-H$) is not possible from the present experiments, since none of the substrates is capable of abstracting an H-atom from CeO_2H^+. However, one can derive $\Delta_F H(CeO_2^+)$ indirectly from the proton affinity and the ionization energy of CeO_2 (Scheme 9). Since reactions of neutral CeO_2 cannot be observed directly in an FT-ICR setup it is necessary to derive the upper bound of the IE and the lower bound of the PA of CeO_2 from the nonoccurrence of the corresponding electron- or proton-transfer reactions with certain

(48) (a) Kappes, M. M.; Staley, R. H. *J. Am. Chem. Soc.* **1981**, *103*, 1286. (b) Buckner, S. W.; Freiser, B. S. *J. Am. Chem. Soc.* **1988**, *110*, 6606. (c) Irion, M. P. *Int. J. Mass Spectrom. Ion Processes* **1992**, *121*, 1. (d) Schröder, D.; Fiedler, A.; Ryan. M. F.; Schwarz, H. *J. Phys. Chem.* **1994**, *98*, 68. (e) Reference 19b. (f) Reference 17d. (g) Stöckigt, D.; Schwarz, H. *Liebigs Ann.* **1995**, 429.

(49) (a) *Gas Phase Ion Chemistry*; Bowers, M. T., Ed.; Academic Press: New York, 1979. (b) *Gaseous Ion Chemistry and Mass Spectrometry*; Futrell, J. H., Ed.; Wiley: New York, 1986.

(50) When small and weakly bound ligands are exchanged, this assumption does not necessarily apply: (a) Schwarz, J.; Heinemann, C.; Schwarz, H. *J. Phys. Chem.* **1995**, *99*, 11405. (b) Heinemann, C.; Schwarz, J.; Schwarz, H. *J. Phys. Chem.*, in press.

(51) (a) Martin, W. C.; Zalubas, R.; Hagan, L. *Atomic Energy Levels—The Rare Earth Elements*, NSRDS-NBS 60; National Bureau of Standards: Washington, DC, 1978. (b) The good agreement between the experimental ionization energy and the result based on density-functional theory may benefit from fortuitous error cancellation since the leading electron configurations, from which the theoretical Kohn−Sham determinants are constructed, contribute less than 60% to the atomic ground states of Ce and Ce^+.

Table 2. Thermochemical Data[a] for CeO_2[b] and CeO_2H

	CeO_2	CeO_2^+	CeO_2H^+
$\Delta_F H$ (kcal/mol)	-147 ± 39	63 ± 31	26 ± 42
IE (eV)	9.1 ± 0.3		

[a] Derived from the present experiments using $\Delta_F H(CeO^+) = 91 \pm 16$ kcal/mol.[44] [b] Earlier experimental values, as recommend by Dyke and co-workers:[44] IE(CeO_2) = 9.7 ± 0.5 eV. $\Delta_F H(CeO_2) = -127 \pm 12$ kcal/mol, thus $\Delta_F H(CeO_2^+) = 73 \pm 23$ kcal/mol.

substrates due to missing exothermicity. While in general the nonobservation of a given reaction may be due to thermodynamic as well as kinetic restrictions, for the special cases of proton- or electron transfers the activation energies are expected to be rather small.[49] As mentioned above, proton transfer is observed from CeO_2H^+ to isobutene (PA(C_4H_8) = 195.9 kcal/mol), while it is absent for toluene (PA($C_6H_5CH_3$) = 189.8 kcal/mol). Thus, PA(CeO_2) amounts to 193 ± 3 kcal/mol. The ionization energy of CeO_2^+ follows from the absence of charge transfer with 1,2,3,4-tetrafluorobenzene (IE = 9.53 eV) and benzene (IE = 9.25 eV), whereas CeO_2^+ is found to abstract an electron from chlorobenzene (IE = 9.07 eV), toluene (IE = 8.82 eV), and *p*-xylene (IE = 8.44 eV). The electron-transfer processes are very inefficient from chlorobenzene and toluene (<5% of all ionic products) suggesting that they occur close to the thermochemical thresholds. However, these electron transfer reactions have to compete with other very efficient reaction pathways (see above) which may influence the accuracy of the bracketing procedure, since the relative efficiencies of oxidation vs hydrogen transfer vs electron transfer pathways may depend on other than thermodynamic influences. Thus, with a conservative error estimate we arrive at IE(CeO_2) = 9.1 ± 0.3 eV, based on the observed charge transfer from chlorobenzene and the nonobservation of electron transfer to benzene. This result leads to BDE(OCe^+O-H) = 89 ± 10 kcal/mol which provides a positive cross-check for the lower bound of the CeO_2^+-H bond strength as derived above. On the other hand, this result suggests that all observed hydrogen-atom abstraction reactions from alkanes proceed closely to their thermodynamic thresholds (see also section VI). These IEs, PAs and BDEs can be converted into heats of formation and these values are summarized in Table 2. The agreement with earlier data for CeO_2 and CeO_2^+, based on appearance potential and equilibrium measurements,[15] is reasonable and justifies the use of the "bracketing" technique for the derivation of thermochemical data.

V. Theoretical Results. From the observed deflection of a molecular beam in an electric quadrupole field[52] and infrared spectroscopic data,[53] the neutral CeO_2 molecule is known to exhibit a bent geometry;[54] experimental information on the structure of its ionic counterpart CeO_2^+ is not available. In this theoretical section, we examine the geometric and electronic structures of these two species and discuss them on the background of the experimental results. To this aim, two different methodologies have been employed. First, the results from quasirelativistic density-functional theory (DFT) are presented, followed by ab initio pseudopotential (PP) calculations and a comparison of these methods. As far as relativistic effects[55] are concerned, the DFT results include an evaluation of the scalar mass−velocity and Darwin terms while the PP calculations investigate the role of spin−orbit effects.

Table 3. Optimized Theoretical Geometries for CeO_2 ($^1\Sigma_g^+$, $^1A_1$) and CeO_2^+ ($^2\Sigma_u^+$)

method		R_e[a]	θ(O−Ce−O)[b]
	CeO_2		
DFT (frozen core)			
LDA + BP	nr[c]	1.800	180.0
	qr[c]	1.843[d,e]	131.5[d,e]
pseudopotential[e]			
HF (A[f])	qr	1.792	116.8
HF (B[f])	qr	1.792	118.1
CISD (A)	qr	1.806	118.1
CISD (B)	qr	1.804	118.8
MRCI (A)	qr	1.813	115.2
ACPF (B)	qr	1.838	117.6
	CeO_2^+		
DFT (frozen core)			
LDA + BP	nr	1.744	180.0
	qr	1.784	180.0
pseudopotential[e]			
HF (A[f])	qr	1.695	180.0
HF (B[f])	qr	1.694	180.0
CISD (A)	qr	1.737	180.0
CISD (B)	qr	1.735	180.0
MRCI (A)	qr	1.756	180.0
ACPF (B)	qr	1.789	180.0

[a] Bond lengths in Å. [b] Bond angles in degrees. [c] Key: nr, nonrelativistic calculation; qr, quasirelativistic calculation. [d] An earlier quasirelativistic Xα calculation yielded R_e(Ce−O) = 1.82 Å and θ(O−Ce−O) = 132°.[63] [e] Spin−orbit effects influence bond lengths by less than 0.01 Å and bond angles by less than 1°. [f] A and B designate the respective basis sets in the pseudopotential calculations.

(a) Density-Functional Calculations. The optimized geometries for CeO_2^+ and CeO_2, calculated within the nonrelativistic and the quasirelativistic density-functional approach, are given in Table 3. *Nonrelativistically*, the neutral CeO_2 molecule adopts a linear geometry. However, upon inclusion of the scalar quasirelativistic treatment, the bond angle θ(O−Ce−O) shrinks to 131.5°, along with an elongation of the cerium−oxygen bond by 0.043 Å. Energetically, the quasirelativistically optimized linear structure (R_e(Ce−O) = 1.850 Å) is only 0.11 eV (2.5 kcal/mol) less stable than the bent equilibrium geometry. Experimentally, θ(O−Ce−O) = 146 ± 2° has been derived based on the infrared spectrum of CeO_2 in an Ar matrix.[53] Note that the latter value does not include corrections for anharmonicity effects (estimated to reduce θ(O−Ce−O) by 5−10°[53]) and the influence of the matrix on the bond angle.

According to the DFT calculations, the cationic CeO_2^+ species exhibits a $^2\Sigma_u^+$ electronic ground state, which arises upon removal of an electron from the $4b_2$ highest molecular orbital of the neutral closed-shell CeO_2 molecule with concomitant relaxation of the O−Ce−O angle to 180°. In this case, both the nonrelativistically and the quasirelativistically optimized geometries are linear. Again, relativity is found to *lengthen*

(52) Kaufman, M.; Muenter, J.; Klemperer, W. *J. Chem. Phys.* **1967**, *47*, 3365.
(53) Gabelnick, S. D.; Reedy, G. T.; Chasanov, M. G. *J. Chem. Phys.* **1974**, *60*, 1167.
(54) For a recent theoretical investigation on the solid state structure of CeO_2, see: Nakamatsu, H.; Mukoyama, T.; Adachi, H. *Chem. Phys. Lett.* **1995**, *247*, 168.
(55) (a) Pyykkö, P. *Chem. Rev.* **1988**, *88*, 563. (b) A comprehensive overview of electronic structure calculations for molecules containing lanthanide atoms is given in a recent review: Dolg, M.; Stoll, H. In *Handbook on the Physics and Chemistry of Rare Earths*; Gschneider, K. A., Eyring, L., Eds.; Elsevier: Amsterdam, 1995; Vol. 22.
(56) (a) Tatsumi, K.; Hoffmann, R. *Inorg. Chem.* **1980**, *19*, 2656. (b) Pyykkö, P.; Lohr, L. *Inorg. Chem.* **1981**, *20*, 1950. (c) Jorgensen, C. K.; Reisfeld, R. *Struct. Bonding* **1982**, *50*, 121. (d) DeKock, R. L.; Baerends, E. J.; Boerrigter, P. M.; Snijders, J. G. *Chem. Phys. Lett.* **1984**, *105*, 308. (g) Pyykkö, J. G.; Laaksonen, L. J.; Tatsumi, K. *Inorg. Chem.* **1989**, *28*, 1801. (h) van Wezenbeek, E. M.; Baerends, E. J.; Snijders, J. G. *Theor. Chim. Acta* **1991**, *81*, 129. (i) van Wezenbeek, E. M. Ph.D. Thesis, Vrije Universiteit Amsterdam 1992. (j) Cornehl, H. H.; Heinemann, C.; Marcalo, J.; de Matos, A. P.; Schwarz, H. *Angew. Chem., Int. Ed. Engl.*, in press.

Table 4. Mulliken Population Analyses of the Metal Valence Orbitals in Quasirelativistic Wave Functions of CeO_2, CeO_2^+, and UO_2^{2+}

	LDA + BP	HF (Basis A)	HF (Basis B)
CeO_2[a]			
6s	1.96 (1.96)	2.05 (2.06)	1.97 (1.96)
5p	5.88 (5.89)	6.01 (5.93)	5.85 (5.69)
5d	1.53 (1.27)	1.87 (1.41)	1.67 (1.26)
4f	1.26 (1.46)	0.82 (1.35)	0.69 (1.26)
q(Ce)	1.38 (1.42)	1.19 (1.19)	1.77 (1.77)
CeO_2^+			
6s	1.92	2.04	1.98
5p	5.63	5.60	5.52
5d	1.16	1.50	1.27
4f	1.34	1.22	1.01
q(Ce)	1.95	1.55	2.17
UO_2^{2+}			
7s	0.00[b]	0.03[c]	
6p	5.39	5.81	
6d	1.08	1.20	
5f	2.58	2.41	
q(U)	3.16	2.54	

[a] At the bent equilibrium geometry. Numbers in parentheses refer to optimized *linear* geometries. [b] $D_{\infty h}$; $R_e = 1.723$ Å (LDA+BP) using a double-ζ polarized basis according to ref 56i. [c] HF results (double-ζ polarized basis) with $R_e = 1.64$ Å taken from ref 57.

the cerium−oxygen bond by a similar order of magnitude (+0.04 Å) as in the neutral counterpart. Relativistic bond lengthening has an interesting parallel in the UO_2, UO_2^{2+},[56] and NUO^+ molecules,[31c] which also exhibit short multiple bonds between an electronegative ligand and a heavy metal. The absolute magnitude of this effect within the same quasirelativistic DFT scheme amounts to +0.044 Å for CeO_2, to +0.040 Å for CeO_2^+ (present work), and to +0.033 Å for UO_2^{2+}.[31c] In the uranium case, the relativistic bond lengthening has been explained by the particular semicorelike nature of the spatially extended uranium 6p shell, which exhibits a hole due to interaction with the 2s valence orbitals of the ligands.[56] The analogy with the cerium dioxide case is evident from the population analyses for the quasirelativistic Kohn-Sham determinants of CeO_2, CeO_2^+, and UO_2^{2+} (Table 4) which give occupations of 5.88 (CeO_2) and 5.63 (CeO_2^+) for the Ce 5p and 5.39 for the U 6p orbitals. The Mulliken population analyses suggest that the hole, which arises upon ionization in the closed-shell species CeO_2, is neither localized on the lanthanide center nor on the oxygen ligands. Removal of an electron increases the Mulliken charge of the cerium atom by 0.57 e with the main contributions from the cerium 5d and 5p orbitals. The remaining 0.43 e are taken from the 2p orbitals on the oxygen ligands. Thus, in CeO_2^+ the unpaired electron resides in the $3\sigma_u$ orbital with contributions from both the oxygen $2p_{z^2}$ and the cerium $4f_{z^3}$, and $5p_{z^2}$ orbitals. In other words, the electronic structure of CeO_2^+ represents neither of the two extremes alluded to in the introduction ($O{=}Ce^{(V)+}{=}O$ vs $O{=}Ce^{(IV)+}{-}O^{\bullet}$); rather, the oxidation state of Ce is best characterized as between IV and V with also radical character at both oxygen atoms in terms of a resonating π-bond.

Theoretical ionization energies for CeO_2 and bond dissociation energies for CeO_2^+ are given in Tables 5 and 6. For the ionization process, we give the adiabatic values as well as the vertical ionization energy of CeO_2 and the vertical electron affinities of CeO_2^+. The absolute difference between the vertical and the adiabatic electron affinities of CeO_2^+ is smaller than for the corresponding vertical and adiabatic ionization energies, reflecting the softer bending potential for the neutral cerium dioxide as compared to the cationic counterpart. Irrespective of the employed functional, relativity decreases the adiabatic

Table 5. Calculated Vertical Ionization Energies (IE_v) for CeO_2, Vertical Electron Affinities (EA_v) for CeO_2^+, and Adiabatic Ionization Energies for CeO_2 (in eV)[c]

method	IE_v	EA_v	IE_a
DFT (frozen core)			
LDA[a]	9.22 (9.02)	8.50 (8.83)	8.65 (8.84)
LDA + B[a]	9.26 (9.11)	8.59 (8.93)	8.89 (9.10)
LDA + BP	9.02 (8.85)	8.31 (8.64)	8.54 (8.76)
pseudopotential[c]			
HF (A)[b]	8.99	7.35	7.80
HF (B)[b]	8.97	7.32	7.75
CISD (A)	9.24	8.07	8.52
CISD (B)	9.34	8.15	8.56
ACPF (A)	9.09	7.85	8.57
ACPF (B)	9.19	7.94	8.61

[a] Using the LDA+BP optimized geometries. [b] A and B designate the respective basis sets in the pseudopotential calculations. [c] Numbers in parentheses refer to nonrelativistic calculations. Spin−orbit effects increase IE_v by 0.05 eV, EA_v by 0.06 eV, and IE_a by 0.05 eV.

Table 6. Calculated Bond Dissociation Energies (BDEs)[a] for $OCe^+{-}O$ (in kcal/mol)[b]

method	BDE
DFT (frozen core)	
LDA[c]	134.1 (113.5)
LDA + B[c]	104.2 (81.0)
LDA + BP	116.9 (95.0)
pseudopotential	
HF (A)	−6.7
HF (B)	−1.6
CISD (A)	61.8
CISD (B)	59.5
ACPF (A)	77.8
ACPF (B)	78.9
CCSD(T) (B)	80.3
exptl	88 ± 15

[a] BDE = $E(CeO_2^+, {}^2\Sigma_u^+) - E(CeO^+, {}^2\Delta$ for DFT methods, $^2\Phi$ for HF, CISD and ACPF) − $E(O, {}^3P)$. [b] Results in parentheses refer to nonrelativistic calculations. The spin−orbit contribution of −10.9 kcal/mol is not included. [c] Using the LDA+BP optimized geometries.

ionization energy of CeO_2 ca. 0.2 eV, as expected from the indirect screening effect,[55] which destabilizes the 5d orbitals of the lanthanide element. The calculated adiabatic ionization energy for CeO_2 using the LDA, LDA+B, and LDA+BP functionals lie well within the present experimental result of 9.1 ± 0.3 eV. For comparison, reasonable agreement is also found for the ionization energy of the cerium atom, which quasirelativistically is calculated as 5.87 eV (LDA), 5.95 eV (LDA+B), and 5.72 eV(LDA+BP), compared to an experimental value of 5.87 eV (corrected for spin−orbit effects by *j*-level averaging for $Ce^+(5d^24f^1, {}^4H)$).[51] As far as the BDE-($OCe^+{-}O$) is concerned, the employed functionals show the well-known overbinding tendency, typical for applications of the employed functionals for open-shell transition-metal systems.[31b−d] Relativity is found to strengthen the $OCe^+{-}O$ bond by ca. 20 kcal/mol. The quasirelativistic LDA+BP result (116.1 kcal/mol) is almost 30 kcal/mol larger than the center of the experimental bracketing result (88 ± 15 kcal/mol) and clearly outside the experimental uncertainties. While LDA without gradient corrections yields an even larger bond energy (134.1 kcal/mol), the LDA+B result (104.2 kcal/mol) is found to be the closest to experiment among all functionals employed here, as already noted for other transition-metal containing open-shell molecules.[31b,c]

Because CeO^+ constitutes one of the fragments in the bond energy calculations, Table 8 summarizes theoretical results on its 4 low-lying ΛS-coupled electronic states. Within the DFT scheme, the ground state of CeO^+ is found to be of $^2\Delta$

Table 7. Calculated Bond Lengths R_e and Adiabatic Term Energies T_e of Low-Lying States of CeO_2^+

	$^2\Sigma_g^+$		$^2\Pi_u$		$^2\Sigma_u^+$		$^2\Pi_g$	
method	R_e (Å)	T_e (eV)	R_e (Å)	T_e (eV)	R_e (Å)	T_e (eV)	R_e (Å)	T_e (eV)
DFT (frozen core)								
LDA + BP	1.890	2.34	1.893	1.51	1.784	0.00	1.930	2.24
pseudopotential								
MRCI (A)	1.872	2.84	1.859	1.82	1.756	0.00 [a]	1.888	3.16
MRCI (B)	1.866	2.88	1.856	1.92	1.750	0.00 [a]	1.880	3.31

[a] The $\Omega = 0.5$ state is lowered by 0.03 kcal/mol with respect to the $^2\Sigma_u^+$ state due to spin−orbit coupling.

Table 8. Calculated Spectroscopic Constants of Low-Lying States of CeO^+ from ΛS-Coupled Calculations

	2Φ		2Δ		2Π		$2\Sigma^+$	
method	R_e (Å)	T_e (cm^{-1})	R_e (Å)	T_e (cm^{-1})	R_e (Å)	T_e (cm^{-1})	R_e (Å)	T_e (cm^{-1})
DFT (frozen core)								
LDA + BP	1.792	2009	1.783	0	1.775	1524	1.778	1453
pseudopotential								
MRCI (A)	1.770	0	1.762	508	1.760	1379	1.760	1288
MRCI (B)	1.768	0	1.760	511	1.760	1380	1.758	1293
ACPF (B)	1.777	0	1.769	580	1.767	931	1.767	1138

symmetry. Electronically, this species is characterized by a "perfect pairing" pattern of the bonding valence electrons plus one single unpaired electron residing in a nonbonding 4f orbital of cerium. Due to the large spin−orbit splitting of the lanthanide 4f levels,[51] we expect a significant spin−orbit stabilization of CeO^+, which might also influence the computed BDEs for CeO_2^+. This aspect will be discussed after the presentation of the ab initio pseudopotential calculations covering spin−orbit coupling further below.

The first electronically excited state of CeO_2^+ has $^2\Pi_u$ symmetry and arises upon removal of an electron from the second highest occupied molecular orbital ($5a_1$) of neutral CeO_2. In this state, the cerium−oxygen bonds are calculated to be ca. 0.1 Å longer than in the $^2\Sigma_u^+$ ground state, and a similar structural trend also applies to the lowest $^2\Pi_g$, and $^2\Sigma_g^+$ states. Energetically, these excited states are more than 1.5 eV disfavored with respect to the ground state. We conclude that, even when a reasonable error estimate of 0.5 eV is attributed to the calculated excitation energies, the theoretical results suggest that the lowest excited states are not accessible within the thermal energy regime. Consequently, the bond and ionization energies for CeO_2^+ and CeO_2, as derived from ion/molecule reactions of thermalized CeO_2^+ cations are not expected to suffer from interference with low-lying electronically excited states and thus represent genuine thermochemical data.

(b) Ab initio Pseudopotential Calculations. The optimized geometries for CeO_2 and CeO_2^+ derived from the quasirelativistic PP calculations are listed in Table 3. Using basis sets A and B, CeO_2 is found to be bent with a bond angle of $117 \pm 2°$ at all levels of theory, i.e. about 15° less than the DFT results. At the MRCI level (basis set A) the linear structure with optimized Ce−O distance is calculated to be 0.36 eV (8.2 kcal/mol) higher in energy, which is by a factor of 3 larger than the energy difference calculated with DFT. The corresponding ACPF value (basis set B) of 0.5 eV (11.5 kcal/mol) is even larger.

CeO_2^+ is found to be linear in all calculations. For both molecules the MRCI bond lengths (basis A) are about 0.03 Å shorter than the corresponding DFT values, whereas the deviations are smaller than 0.01 Å for the ACPF values. Similar trends are observed for CeO^+ (Table 8). The differences between the PP configuration interaction and the DFT calculations might be due to basis set effects: PP HF calculations with basis sets of valence double-ζ quality yield a bond angle of 137° for CeO_2 as well as bond lengths of 1.828 and 1.772 Å for CeO_2 and CeO_2^+, respectively. Reducing the size of the 5d(Ce) and the 2s, 2p (O) basis in the DFT calculations (LDA+BP functional) to double-ζ quality also leads to a larger O−Ce−O angle (147.5°) and longer cerium−oxygen bonds (1.860 Å) for CeO_2. Finally, spin−orbit effects influence the bond lengths and bond angles by less than 0.01 Å and 1°, respectively. The energy difference between bent and linear CeO_2 is decreased by merely 0.01 eV (0.2 kcal/mol).

The bent equilibrium geometry of CeO_2 needs some further comments. The Mulliken population analyses summarized in Table 4 suggest that a balanced d and f basis set is needed to obtain reliable data for the CeO_2 bond angle. Bent and linear structures are favored by 6s/5d and 6s/4f hybridization on Ce, respectively.[57] Since there is no excplicitly occupied Ce 4f orbital in CeO_2, one may evaluate the influence of the 4f shell on the O−Ce−O angle by omitting the f-functions in the basis set. As expected from the hybridization argument, we find that at the HF level the bond angle is reduced by 12° and the bond length decreases by 0.08 Å. Moreover, the energy difference between the bent equilibrium geometry and the linear geometry is increased by 2.30 eV (53.0 kcal/mol). Thus, f-functions are essential for describing the structural properties of CeO_2, but it is difficult to deduce from these results whether this is a polarization or a genuine hybridization effect.

In earlier work, Wadt attributed the structural differences between ThO_2, the bent actinide homolog of CeO_2, and the linear isoelectronic uranyl dication UO_2^{2+} to the different ordering of the 5f and 6d orbitals of the actinide atoms.[57] The 5f orbitals are lower in energy than the 6d orbitals and dominate back-bonding from oxygen in UO_2^{2+}, whereas the opposite is true for ThO_2. We note here that a discussion in terms of orbital energies alone may be misleading for the 4f-elements: In Ce^{2+} ($4f^15d^1$) the difference between the orbital energies of the 4f (−1.00 au) and 5d (−0.68 au) orbitals is almost a factor of 2 larger than the one given by Wadt for the respective levels of U^{2+} ($5f^36d^1$; 5f, −0.80 au; 6d, −0.64 au); nevertheless, CeO_2 is bent whereas UO_2^{2+} is linear. On the other hand, for estimating the efficiency of orbitals in chemical bonding, one also has to consider an additional criterion, their radial extent. The ratio of the radial expectation values of Ce^{2+} 5d (2.57 au) and 4f (1.03 au) is 2.50, whereas the one for U^{2+} 6d (2.79 au) and 5f (1.42 au) is 1.96. Thus, the more compact nature of the lanthanide 4f orbitals as compared to the actinide 5f orbitals makes their participation in bonding less favorable in terms of overlap with ligand orbitals such as those of oxygen in the present case and 5d/6s rather than 4f/6s hybridization determines the bent equilibrium geometry of CeO_2.

The calculated CISD and ACPF ionization energies of CeO_2 (Table 5) show the same qualitative trend ($IE_v > IE_a > EA_v$) as the DFT results. Spin−orbit effects are again of minor importance and increase all calculated ionization energies and electron affinities marginally (IE_v, +0.05 eV; IE_a, +0.05 eV; EA_v, +0.06 eV). Quantitatively, the correlated PP methods yield ionization energies which deviate by less than 0.5 eV from the DFT results and are in excellent agreement with the experimental value.

In order to estimate $BDE(OCe^+-O)$, calculations within the ΛS and intermediate (including spin−orbit effects) coupling schemes for the low-lying electronic states of CeO^+ were

(57) Wadt, W. R. *J. Am. Chem. Soc.* **1981**, *103*, 6053.

Table 9. Calculated Spectroscopic Constants[a] of Low-Lying States of CeO^+ from MRCI Calculations in the Intermediate Coupling Scheme (Basis set C), Where Ω Is the Total Angular Momentum Quantum Number

Ω	R_e (Å)	T_e (cm^{-1})
2.5	1.795	0
1.5	1.788	404
0.5	1.788	1164
3.5	1.796	2291
2.5	1.789	2491
1.5	1.788	3232
0.5	1.788	3421

[a] The vibrational constants are (1000 ± 1) cm^{-1} for all states ((999 ± 1) cm^{-1} without spin−orbit coupling). The Ω = 2.5 state is lowered by 11.6 kcal/mol with respect to the $^2\Phi$ state due to spin−orbit coupling.

required. These results are summarized in Tables 8 and 9 and supplement earlier data for neutral CeO,[58] which are in good agreement with the available experimental data.[59] The agreement between the ab initio PP and the DFT results with respect to the geometries and term energies of the $^2\Delta$, $^2\Pi$, and $^2\Sigma^+$ states of CeO^+ is reasonable, and the deviations between the two methods remain within the expected range. However, in the PP calculations the $^2\Phi$ state is found to be the ground state of CeO^+, at variance with the DFT method, which predicts this state to be the energetically least favorable of all four low-lying states considered here. A similar behavior is found for the DFT-computed relative energies of the $^1\Phi$ and $^3\Phi$ states within the low-lying state manifold of neutral CeO. Since the ground state of CeO is experimentally known to exhibit $^3\Phi$ symmetry[59] with the singly occupied 6s orbital as HOMO,[58] a $^2\Phi$ ground state for the CeO^+ cation is intuitively reasonable, and this expectation is corroborated by our ab initio PP calculations. However, the unreasonably high relative energy of this state within the DFT scheme is unsatisfactory and calls for more detailed investigations, which are not purpose of the present work.

As expected, the bond dissociation energies for CeO_2^+ as derived from the correlated PP calculations are lower than the corresponding DFT results (Table 6). With respect to experiment, the best value obtained with the size-consistent ACPF method and basis set B (78.9 kcal/mol) is within the experimental bracketing result (88 ± 15 kcal/mol). However, in the PP calculations it is found that spin−orbit effects lower the energies of CeO_2^+ and CeO^+ by 0.7 kcal/mol (Table 7) and 11.6 kcal/mol (Table 9), respectively. Neglecting the small spin−orbit effects on the oxygen atom, we may estimate that the spin−orbit corrected ACPF result is 68.0 kcal/mol. Bond lengths and term energies of the low-lying excited states of CeO_2^+ are given in Table 7. At the MRCI level, the first excited $^2\Pi_u$ state is 2.20 eV above the $^2\Sigma_u^+$ ground state, in good agreement with the LDA+BP result of 1.91 eV. The qualitative and quantitative agreement becomes, however, somewhat worse for the higher excited states.

(c) Comparison. To summarize this section, we have found reasonable agreement between gradient-corrected density functional and correlated ab initio pseudopotential calculations as far as the electronic and geometric structures as well as ground state energetic properties of CeO_2 and CeO_2^+ are concerned. With respect to the binding energy of an oxygen atom to CeO^+, the spin−orbit corrected ACPF calculation yields a result 5 kcal/mol smaller than the lower limit of the experimental bracketing result (88 ± 15 kcal/mol). Adding the same spin−orbit correction to the DFT results, we obtain BDE(OCe^+−O) as 93.3 kcal/mol (LDA+B) and 106.0 kcal/mol (LDA+BP), respectively. Thus, for the first cerium−oxygen binding energy in CeO_2^+ the LDA+B functional compares most favorably among all methods considered here. With all methods (expect for HF), the calculated ionization energies of CeO_2 are within the experimental bracketing value of 9.1 ± 0.3 eV. Thus, as far as the application of density-functional methods for the theoretical description of ground state electronic properties of small lanthanide complexes is concerned, one is led to a positive conclusion. Although it may in certain cases be difficult to recognize potential pitfalls of these methods (primarily, these seem to appear in the treatment of excited states, see the discussion of CeO^+), the geometric and energetic properties at least of systems as complex as CeO_2^+ might be expected to be well reproduced if one regards highly correlated ab initio results and available experimental data as reference marks.

Table 10. Rate Constants Relative to the Theoretical Collision Rate Constant k_{ADO}[25] for C−H Bond Activation of Saturated and Unsaturated Hydrocarbons by CeO_x^+ cations ($x = 0-2$)

	Ce^+	CeO^+	CeO_2^+
CH_4	< 0.001[a]	< 0.001	< 0.001
C_2H_6	0.001[a]	< 0.001	< 0.001
C_3H_8	0.15[a]	< 0.001	0.003
n-C_4H_{10}	0.40[a,b]	< 0.001	0.10
i-C_4H_{10}	0.20[a,b]	< 0.001	0.04
neo-C_5H_{12}	0.01[b]	< 0.001	0.03
c-C_6H_{12}	0.80[a]	< 0.001	0.35
C_2H_4	1.00	< 0.001	0.10
$CH_2{=}CHCH_3$	1.00[a,b]	< 0.001	0.44
$CH_2{=}CHCH_2CH_3$	1.00[b]	< 0.001	0.62
$CH_2{=}CHCH{=}CH_2$	1.00[b]	< 0.001	0.80
C_6H_6	1.00	< 0.001	0.64

[a] Reference 11g. [b] Also C−C bond activation reactions occur.

VI. Comparison of Ce^+, CeO^+, and CeO_2^+ in their Reactions with Hydrocarbons. Table 10 lists the rate constants measured for "bare" Ce^+, CeO^+, and CeO_2^+ with a common set of saturated and unsaturated hydrocarbons. Most of the information for Ce^+ is taken from an earlier study[11g] and has been supplemented by the data for Ce^+/neopentane, Ce^+/ethene, Ce^+/1-butene, Ce^+/butadiene, and Ce^+/benzene systems for the present purpose.[60] In contrast to Ce^+ and CeO_2^+, the cationic cerium monoxide CeO^+ was found to be completely unreactive with all substrates considered here (except for slow adduct formation, which is not discussed here). To understand the different reaction patterns, we focus on the general potential energy surface of an ion/molecule reaction as displayed in Figure 2. The initial step of such a process is the formation of a weakly bound adduct complex between the metal complex ML^+ (L = ligand) and the substrate S, which remains rovibrationally excited under single colllision conditions. Most generally, one or more transition states (TS) have to be passed en route to the electrostatic adduct between the product metal complex ML'^+ and the eventually lost neutral product P. The efficiency of the overall process depends on the interplay of several factors such as the lifetimes of the primary adduct complexes, the heights of the barriers and the relative energies of the entrance and exit channels.[61]

(58) Dolg, M.; Stoll, H.; Preuss, H *J. Mol. Structure (THEOCHEM)* **1991**, *231*, 243.
(59) Linton, C.; Dulick, M; Field, R. W.; Carette, P.; Leyland, P. C.; Barrow, R. F. *J. Mol. Spectrosc.* **1983**, *102*, 441.
(60) The product distributions are: (a) Ce^+/neopentane: $CeC_4H_6^+$, 100% (loss of $CH_4 + H_2$). (b) Ce^+/ethene: $CeC_2H_2^+$, 100% (loss of H_2). (c) Ce^+/1-butene: $CeC_4H_6^+$, 80% (loss of H_2); $CeC_4H_4^+$, 10% (loss of 2 H_2); CeC_2H_2, 10% (loss of C_2H_6). (d) Ce^+/butadiene: $CeC_4H_6^+$, 15% (adduct formation); $CeC_4H_4^+$, 30% (loss of H_2); $CeC_2H_2^+$, 55% (loss of C_2H_4).
(61) Tolbert, M. A.; Beauchamp, J. L. *J. Am. Chem. Soc.* **1986**, *108*, 7509.

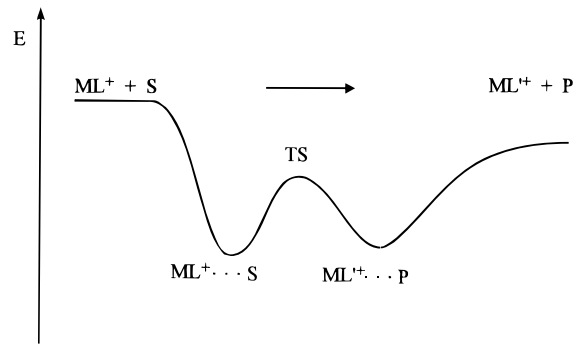

Figure 2. General potential energy surface for an ion/molecule reaction.

In reactions of "bare" Ce^+ cations with hydrocarbons, intact closed shell molecules such as H_2, C_2H_4, or C_2H_6 are lost exclusively with a general preference for C−H over C−C bond activation processes. In earlier studies[11d,g] we have shown that a "classical" mechanism involving the insertion of Ce^+ (which has three unpaired electrons in the $5d^24f^1$ ground state configuration) into a weak C−H bond of the hydrocarbon followed by rearrangements via e.g. β-hydrogen shifts and finally losses of H_2 or small hydrocarbons can account for these processes. It could be shown that the non-occurrence of a reaction between Ce^+ and methane is due to endothermicity (i.e. the product channel is energetically disfavored with regard to the reactants). Moreover, the increasing rates along the series propane, isobutane, cyclohexane, and propene were accounted for by the increase in polarizabilities (stabilizing the primary adduct complexes), the decreasing strengths of the weakest C−H bonds in these systems (which should lower the relative energies of the respective TSs), and the increasing thermodynamic driving forces (which lower the relative energies of the exit channels). The present data are in qualitative agreement with these arguments. For example, the low efficiency of the Ce^+/neopentane reaction is easily rationalized by the presence of only strong primary C−H bonds in this system and the missing possibility for a "simple" β-hydrogen migration which requires either rearrangements of the carbon skeleton or a multicenter transition state on the way to the observed product ion $CeC_4H_6^+$. On the other hand, the corresponding activations of ethene, 1-butene, butadiene, and benzene are kinetically efficient due to the larger attractive ion/substrate interaction potentials and the presence of themodynamically favorable product channels.

In the light of these data, the inability of CeO^+ to activate any of the considered substrates is most probably due to thermodynamic restrictions. According to the theoretical data, CeO^+ possesses a single unpaired electron residing in a spatially compact and "chemically inactive"[11] 4f-orbital of cerium. Thus, insertion of this species into a C−H bond of R−H requires formal fission of the strong cerium−oxygen bond. The resulting hypothetical cationic alkyl−hydrido−oxy cerium species (H)(R)CeO^+ involves a substantially weakened cerium−oxygen interaction and is expected to be destabilized with respect to the entrance channel compared to the analogous process with the "bare" Ce^+ cation. Similar arguments apply for the possible addition of a substrate across the Ce−O bond, i.e. ions of the $H-Ce-OR^+$ or $R-Ce-OH^+$ connectivities. For comparison, the attachment of a second oxygen atom to CeO^+, as shown in the present work, requires a strong oxidation reagent (NO_2), and is driven by the delocalization of the unpaired electron along the O−Ce−O linkage. The same stabilization is, however, not expected for (H)(R)CeO^+ since the hydrogen and alkyl ligands require a perfect pairing pattern of the electrons involved in the respective bonds to cerium. Finally, we point out that also a direct hydrogen abstraction pathway resulting in the formation of $HCeO^+$ and a hydrocarbon radical is expected to be thermodynamically unfavorable since the $H-CeO^+$ bond is probably much weaker than any C−H bond in the substrates considered here due to the 4f-character of the unpaired electron in CeO^+.

Finally, let us focus on CeO_2^+. The reactivity of this species toward the present set of substrates is intermediate between "bare" Ce^+ and CeO^+. For the comparison between Ce^+ and CeO_2^+, we will concentrate on the C−H bond activation reactions, since oxidation of the substrates is not an issue for the cerium cation itself. At first, for most substrates the reactions of alkanes with CeO_2^+ are less efficient as compared to Ce^+ and proceed mostly via hydrogen abstraction to yield CeO_2H^+ and neutral hydrocarbon radicals. H-atom abstraction is not observed for "bare" Ce^+ cations and points to a different mechanism being operative in the CeO_2^+/alkane systems. According to its electronic structure, CeO_2^+ has one single unpaired electron. Thus, insertion into C−H or even C−C bonds is expected to be disfavored on the basis of the arguments given for CeO^+. On the other hand, the $OCeO^+-H$ bond strength amounts to 89 ± 10 kcal/mol, which renders activation of methane (BDE(H_3C-H) = 105 kcal/mol) endothermic, in accord with our observation. The primary and secondary C−H bond energies for all other alkanes considered here amount to 99 ± 1 kcal/mol. Thus, these processes must proceed close to their thermochemical thresholds. In such a situation, for a given C−H bond strength, the lifetime of the primary ion/molecule complexes will determine the efficiency of the activation reaction and this explains the non-occurrence of ethane activation (BDE(C_2H_5-H) = 100 kcal/mol) compared to the corresponding process involving propane (BDE(*i*-C_3H_7-H) = 99 kcal/mol vs BDE(*n*-C_3H_7-H) = 101 kcal/mol). However, even a substrate as polarizable as cyclohexane reacts only in 35% of all collisions. This is consistent with the view that, as the radical abstraction type C−H bond activation proceeds at the thermochemical threshold, one expects a maximum of 50% reaction efficiency if no barriers are present (thermoneutral ligand exchange[11d]) and even less in a process involving an intermediate TS.

The rise of the reaction efficiencies along the sequence C_3H_8 < *neo*-C_5H_{12} < *i*-C_4H_{10} < *n*-C_4H_{10} < *c*-C_6H_{12} can be rationalized by the number of easily activated C−H bonds. Obviously, C−C bond activation is not observed for CeO_2^+. The distinct observation of $CeO_2H_2^+$ as a primary product ion in the CeO_2^+/cyclohexane system compared to all other alkanes (see above) can be accounted for by larger lifetimes of the product complexes such that a second hydrogen atom may be transferred ($[CeO_2H^+-C_6H_{11}^{\bullet}] \rightarrow [CeO_2H_2^+-C_6H_{10}] \rightarrow CeO_2H_2^+ + C_6H_{10}$). For CeO_2^+/isobutane, $CeO_2H_2^+$ may evolve after the primary C−H bond activation as a subsequent cleavage of the weak tertiary C−H bond (BDE($(H_3C)_3C-H$) = 95 kcal/mol), i.e. $CeO_2^+ + i\text{-}C_4H_{10} \rightarrow [CeO_2H^+-((CH_3)_2CHCH_2^{\bullet})] \rightarrow CeO_2H_2^+ + (CH_3)_2C{=}CH_2$. In this view, $CeO_2H_2^+$ is not observed as a primary product in the CeO_2^+/*n*-butane system because only stronger primary and secondary C−H bonds are present in this substrate.

The low reaction efficiencies for the CeO_2^+/alkane reactions are somewhat surprising as compared to those of the reactions of CeO_2^+ with unsaturated hydrocarbons. As a possible explanation, we propose relatively low complexation energies of CeO_2^+ with alkanes and hence kinetic and thermochemical restrictions are associated with the activation of C−H bonds. For example, based on DFT calculations with the methods employed for the present study, we estimate the depth of the CeO_2^+/CH_4 interaction potential as ca. 6 kcal/mol compared to

ca. 20 kcal/mol for "bare" Ce^+ with CH_4.[62] Note that the BDEs(C−H) of the alkanes are 10−15 kcal/mol higher than those in the olefins bearing allylic C−H bonds, for which fast C−H activations are observed. A similar thermochemical argument applies for the oxygen transfer, e.g. hydroxylation of ethane by CeO_2^+ to yield ethanol is exothermic by 8 ± 15 kcal/mol while in the case of ethylene 25 ± 15 kcal/mol are released if the thermodynamically most stable product (acetaldehyde) is formed. The influence of possible energy barriers for the oxidation reactions is not easy to estimate without detailed knowledge of the underlying potential energy surfaces. However, one can account for the different rate constants considering that oxidation of a double bond should be kinetically easier than that of an unfunctionalized alkane because the former substrate allows a facile cycloaddition/cycloreversion type of mechanism whereas several consecutive bond fission and bond formation steps are usually involved in the hydroxylation process.[5]

Summary and Conclusions

The main results of this study can be summarized as follows. (*i*) CeO_2^+ can be generated in an exothermic ion/molecule reaction from CeO^+ and NO_2. (*ii*) The CeO_2^+ cation serves as an oxygen atom donor to a variety of unsaturated hydrocarbon substrates and cyclohexane. Catalytic oxidation of ethene by NO_2 is mediated by CeO_2^+. Under the experimental conditions, the turnover number is limited to 8 because of side reactions with background contaminants. (*iii*) Effective C−H bond-activation of unsaturated allyl-type hydrocarbons is effected by CeO_2^+ with formation of the $CeO(OH)^+$ complex. The corresponding reactions with saturated hydrocarbons are found to be much slower. (*iv*) Bracketing experiments yield the following thermochemical data: $\Delta_F H(CeO_2) = -147 \pm 39$ kcal/mol; $\Delta_F H(CeO_2^+) = 63 \pm 31$ kcal/mol; $\Delta_F H(CeO_2H^+) = 26 \pm 42$ kcal/mol, $PA(CeO_2) = 193 \pm 3$ kcal/mol, $IE(CeO_2) = 9.1 \pm 0.3$. (*v*) According to quasirelativistic ab initio pseudopotential and density-functional calculations and in accord with the experimental data CeO_2^+ is characterized as a linear molecule in which the Ce^+ cation is formally inserted into an O_2 molecule. Its ground state ($^2\Sigma_u^+$) electronic structure, as intermediate between Ce(V) and Ce(IV), is well described by the density-functional and ab initio pseudopotential methods. Relativity is found to lengthen the Ce−O bonds and to strengthen them by ca. 20 kcal/mol. (vi) The presence of the two oxygen ligands in CeO_2^+ induces a change in the mechanism for C−H bond activation with respect to the "bare" Ce^+ cation from the insertion/elimination type to direct hydrogen abstraction. Low efficiencies for CeO_2^+/alkane reactions can be rationalized on the basis of thermodynamic restrictions as well as short lifetimes of the encounter complexes. CeO^+, on the other hand, is completely unreactive toward simple saturated and unsaturated hydrocarbons.

In conclusion, we hope to have demonstrated that ligand effects in the gas-phase chemistry of lanthanide cations can be substantial. For smaller systems, as in the present case, they may be rationalized in combination with theoretical methods for the analysis of geometries and electronic structures. The observed oxo ligand effects are not additive in the sense that a first oxygen atom almost completely switches off the ability of Ce^+ to activate C−H bonds in hydrocarbons while the second oxo ligand increases it again with a concomitant change of the mechanism. For theoretical purposes, density-functional theory appears as a practical tool for the treatment of small 4f-element complexes. While problems in the treatment of excited states may occur, the overall quantitative accuracy is close to the computationally much more expensive ab initio methods. Finally, it should be kept in mind that in the future larger systems involving lanthanide elements need to be approached from the theoretical point of view. This will require methods by which meaningful results can be obtained at reasonable computational efforts and DFT seems to be very promising in this respect.

Acknowledgment. The authors would like to thank Dipl.-Chem. Heike Friedrichs for helpful discussions. Financial support by the Deutsche Forschungsgemeinschaft (Schwerpunktprogramm "Relativistische Effekte"), the Fonds der Chemischen Industrie (Kékulé-Fellowships for C.H. and H.H.C.), the Volkswagen Stiftung (Schwerpunktprogramm "Elektronentransfer"), and the European Science Foundation (REHE Program) is gratefully acknowledged. M.D. thanks the Ohio Supercomputer Center for providing computer time and R. M. Pitzer for his hospitality during a stay at the Ohio State University.

IC951322K

(62) Heinemann, C.; Cornehl, H. H.; Schwarz, H. unpublished theoretical results. Calculated structures and energies for the Ce^+/CH_4 and CeO_2^+/CH_4 complexes are available upon request from the authors. e-mail: schw0531@zrzsp5.chem.tu-berlin.de.

(63) DeKock, R. L.; Peterson, M. A.; Timmer, L. K.; Baerends, E. J.; Vernooijs, P. *Polyhedron* **1990**, *9*, 1919.